PAPER • **OPEN ACCESS**

Surfactant-free gold nanostars as a colloidal substrate for the surface-enhanced Raman spectroscopy of grouper epidermal mucus

To cite this article: Nathaniel Leong *et al* 2025 *Nanotechnology* **36** 435501

OPEN ACCESS
IOP Publishing
Nanotechnology

Nanotechnology **36** (2025) 435501 (14pp)
https://doi.org/10.1088/1361-6528/ae0ada

Surfactant-free gold nanostars as a colloidal substrate for the surface-enhanced Raman spectroscopy of grouper epidermal mucus

Nathaniel Leong[1], Chou Min Chong[2], Annie Christianus[3], Zuraidah Zan[1], Mohammed Thamer Alresheedi[4], Norita Mohd Yusoff[5], Mohd Hanif Yaacob[1] and Mohd Adzir Mahdi[1,6,*]

[1] Wireless and Photonics Networks Research Centre, Faculty of Engineering, Universiti Putra Malaysia, 43400 Serdang, Selangor, Malaysia
[2] Laboratory of Sustainable Aquaculture (AquaLab), International Institute of Aquaculture and Aquatic Sciences (I-AQUAS), Universiti Putra Malaysia, 70150 Port Dickson, Negeri Sembilan, Malaysia
[3] Department of Aquaculture, Faculty of Agriculture, Universiti Putra Malaysia, 43400 Serdang, Selangor, Malaysia
[4] Department of Electrical Engineering, College of Engineering, King Saud University, PO Box 800, Riyadh 11421, Saudi Arabia
[5] School of Optoelectronic Engineering, Xidian University, Xi'an 710071, People's Republic of China
[6] Institute of Nanoscience and Nanotechnology (ION2), Universiti Putra Malaysia, 43400 Serdang, Selangor, Malaysia

E-mail: mam@upm.edu.my

Received 20 June 2025, revised 14 September 2025
Accepted for publication 24 September 2025
Published 24 October 2025

Abstract

Surface-enhanced Raman spectroscopy (SERS) is an emerging analytical method for biological analysis, leveraging the 'lightning rod' effect of metallic nanostructures to intensely amplify signals. Gold nanostars, with their numerous sharp tips, are particularly effective SERS substrates. In this work, biocompatible gold nanostars without harmful surfactants were synthesised using silver ions to control spike formations. Gold nanostars were investigated as a colloidal SERS substrate for the in-solution analysis of grouper epidermal mucus, a key indicator of fish health. The morphology of the gold nanostars was tuned by varying the concentration of silver nitrate ($AgNO_3$) from 0.5 to 3 mM. It was found that an increase in $AgNO_3$ led to higher spike density but shorter, lower aspect ratio spikes. Gold nanostars synthesised with 1 mM $AgNO_3$ produced the highest aspect ratio (3.25) and were shown to exhibit the strongest SERS enhancement. This was validated across various analytes, including

* Author to whom any correspondence should be addressed.

rhodamine 6G (R6G), lysozyme and the grouper epidermal mucus itself. The enhancement factor of 4.72×10^6 and 7.62×10^5 were obtained with R6G and lysozyme, respectively. Ultimately, gold nanostars with long spikes were proven to be superior for in-solution SERS, achieving an enhancement factor two orders of magnitude higher than that of spherical gold nanoparticles in our previous work.

Supplementary material for this article is available online

Keywords: surface-enhanced Raman spectroscopy, gold nanostars, fish mucus

1. Introduction

Raman spectroscopy is an analytical method where the shift in the wavelength of the scattered light from a material is used to measure the vibrational energy of the material. Chemical and structural information of a material can be obtained from the Raman spectrum [1]. Advancements in detector technology, optical filters, laser diodes and optical fibre coupling have allowed routine Raman analysis [2]. Surface-enhanced Raman spectroscopy (SERS) is developed to address two major challenges in Raman spectroscopy, namely; low signal intensity and fluorescence interference [3].

Typically, SERS substrates are fabricated by immobilising metallic nanostructures on solid substrates [4–6]. A recent study has reported the application of solid SERS substrates for the detection of breast cancer using blood plasma [7]. However, the fabrication process of solid SERS substrates can be complex, expensive, labour and time consuming. On the other hand, in-solution SERS using gold nanoparticle colloid is a relatively straightforward, cost-efficient, and rapid method for biomaterial analysis. In a colloidal system, the Raman scattering of the molecules in the vicinity of the metallic nanoparticles [8] is enhanced through the generation of strong localised surface plasmon resonance (LSPR) in the narrow interparticle gap of the nanoparticles [9], which can be tuned using salt-induced aggregation [10].

Anisotropic gold nanoparticles, particularly gold nanostars, have gained interest as colloidal SERS substrates due to their intense electromagnetic field localised at the sharp edges [11]. Due to their unique morphology, the SERS enhancement factor of gold nanostars can outperform that of spherical gold nanoparticles [12]. There are three approaches to synthesise gold nanostars, namely; seed-mediated growth using surfactant, seedless approach using surfactant and surfactant-free approach [13]. Some examples of surfactants used include cetyltrimethylammonium bromide (CTAB) or chloride, sodium dodecyl sulphate and polyvinylpyrrolidone [14]. The use of surfactants reduces the SERS performance of the gold nanostars [15] and the cytotoxic nature of some surfactants such as CTAB [16] limits their use in biological applications.

Therefore, surfactant-free gold nanostars are more biocompatible. The synthesis route begins with citrate-capped gold nanoparticles seed as the core. Anisotropic growth is mediated by silver ions which selectively binds to certain facets of the core, inhibiting growth on that facet. Thus, leading to the formation of spikes radiating outwards from the core. Some biological applications of surfactant-free gold nanostars include its use as a contrast agent for imaging [17], 3D modelling and two-photon luminescence imaging [18]. Surfactant-free gold nanostars are promising in SERS applications due to the high detection sensitivity down to single molecule detection [19] and has been applied in the detection of uranyl [20] and paraquat residue in green tea [21].

Fish epidermal mucus is secreted by the goblet and sacciform cells on the epidermis [22] and is an important component of the innate immune defence against pathogens. Antimicrobial compounds such as proteases, lectins, lysozyme, antimicrobial peptides, and proteins are found in fish epidermal mucus [23]. Nurhikmah *et al* [24] found that the proteomic profile of hybrid grouper (*Epinephelus fuscoguttatus* × *Epinephelus lanceolatus*) change in response to *Vibro alginolyticus* infection. Therefore, a detailed understanding of the epidermal mucus constituents can provide valuable insight into fish health. We have previously studied hybrid grouper epidermal mucus using SERS with spherical citrate-capped gold nanoparticles with acidified sodium sulphate (Na_2SO_4) as the aggregating agent [25]. Surfactant-free gold nanostars are particularly attractive in the application of SERS analysis of grouper epidermal mucus due to its higher sensitivity. Therefore, in this work, we explore surfactant-free gold nanostars as a potential colloidal substrate to enhance the SERS analysis of grouper epidermal mucus.

2. Methodology

2.1. Materials and reagents

Gold (III) chloride trihydrate crystals ($HAuCl_4$, ACS reagent grade) and silver nitrate ($AgNO_3$, ACS reagent grade) were purchased from Sigma-Aldrich. 0.5 g of the $HAuCl_4$ crystals were dissolved in 10 ml of deionised water to obtain the stock solution. Similarly, a 100 mM stock solution of $AgNO_3$ was prepared by dissolving the appropriate amount of the solid in 10 ml of deionised water. The stock solutions were stored in a brown bottle in the refrigerator at 4 °C. Sodium citrate dihydrate ($Na_3Ct{\cdot}2H_2O$, USP testing specifications), L-ascorbic acid (ACS reagent grade), sodium sulphate (Na_2SO_4, ACS reagent grade), lysozyme from hen egg white and rhodamine 6G (R6G, 99% pure) were purchased

from Sigma-Aldrich. All syntheses were carried out in deionised water. An appropriate amount of Na_2SO_4 was dissolved in deionised water to achieve a series of concentrations of 2, 1, 0.5, 0.25 and 0.1 M. The final pH level of the aggregating agents was adjusted to pH 3 using 1% sulphuric acid (H_2SO_4) solution. Similarly, 300 μg ml^{-1} of lysozyme and 0.1 mM of R6G solution were prepared by mixing an appropriate amount of lysozyme and R6G solution in deionised water, respectively.

2.2. Characterisation of gold nanoparticles

The characterisation of gold nanoparticles and gold nanostars was performed using UV-visible spectroscopy (Lambda 35, Perkin Elmer) and transmission electron microscopy (TEM, JEOL JEM-2100F Field Emission TEM). The UV-visible absorption spectra of the gold nanoparticle seed and gold nanostars were measured in a 1 cm $\times$ 1 cm quartz cuvette in a dual-beam setup. About 10 μl of the gold nanoparticle seed and gold nanostars colloid were dropped onto a carbon-coated copper TEM mesh grid and allowed to dry overnight before TEM imaging. A 400-mesh, 3 mm carbon- and formvar-coated copper grid was used for TEM imaging. The dimensions of the gold nanostars were measured from the TEM image using the image processing software ImageJ (version 1.54). Dynamic light scattering (DLS, Zetasizer Nano-S, 633 nm, Malvern Panalytical) was performed to measure the hydrodynamic diameter and size distribution of the gold nanostars.

2.3. Preparation of gold nanoparticles seed

Spherical citrate-capped gold nanoparticles were used as the seed for the subsequent preparation of the gold nanostars. The gold nanoparticle seeds were prepared using the citrate reduction method [26]. The stock $HAuCl_4$ solution was diluted to 1 mM in a volume of 20 ml, which was subsequently heated to 100 °C under rapid stirring at 500 rpm. At 100 °C, 3 ml of 1% Na_3Ct solution was quickly added to the gold precursor. The colour of the solution changed from pale yellow to dark purple and subsequently turned deep red, which indicates the formation of gold nanoparticles. The heating was maintained for 30 min to ensure the reaction was complete. This process yielded 16 nm citrate-coated spherical nanoparticles. The resulting colloid was allowed to cool to room temperature and then deionised water was added until the final volume reached 20 ml to compensate for solvent loss during the synthesis process. The colloid was subsequently stored in a brown bottle in the refrigerator at 4 °C until needed.

2.4. Surfactant-free synthesis of gold nanostars

The surfactant-free synthesis of gold nanostars in this work followed the procedure outlined by Yuan *et al* [18]. The stock $HAuCl_4$ solution (pH 3) was diluted to 0.25 mM in a total volume of 10 ml. Next 100 μl of the seed solution was added. The vial containing the gold precursor was placed into an ice bath, and stirring was initiated at 750 rpm. The synthesis was carried out at 5 °C to improve the reproducibility [27]. When the temperature of the solution reached 5 °C, 100 μl of $AgNO_3$ solution and 50 μl of 100 mM ascorbic acid solution were added simultaneously. To obtain gold nanostars with various shapes, several batches were synthesised using $AgNO_3$ solution with concentrations of 3, 2, 1 and 0.5 mM. The simultaneous addition of $AgNO_3$ and ascorbic acid was crucial to form the gold nanostars. If $AgNO_3$ is added to silver chloride (AgCl) at an early stage causes further precipitation, if it is added too late, spherical gold nanoparticles will form in the presence of ascorbic acid [18]. Immediately after the addition of $AgNO_3$ and ascorbic acid, the colour of the solution changed from pale pink to dark blue. The stirring was maintained for 30 s, and the resulting colloid was centrifuged immediately at 3500 rpm for 15 min to quench the reaction. The resultant pellet containing the gold nanostars was redispersed in 10 ml of deionised water. The final pH of all synthesised gold nanostars was kept at 6.5.

2.5. Mucus sample collection

The procedure for grouper epidermal mucus was performed as previously described [25]. Briefly, juvenile hybrid grouper (*Epinephelus fuscoguttatus* $\times$ *Epinephelus lanceolatus*) measuring about 5 inches in length was transferred to a 25-litre aquarium filled with seawater. In this work, 100 ppm of tricaine methanesulfonate was added to the aquarium as an anaesthesia for easier handling of the fish during mucus sample collection. The fish was left in the aquarium for a few minutes until it showed minimal movement. The epidermal mucus was scraped from head to tail on both sides into a 1.5 ml centrifuge tube, carefully avoiding any blood or urogenital secretion. After mucus sampling, the fish was transferred to another aquarium until the effects of the anaesthesia wore off and then returned to the culture tank. The mucus samples were homogenised briefly using an ultrasonic sonotrode and then centrifuged at 5000 rpm for 5 min to separate the debris. The debris-free mucus samples were aliquoted into new 1.5 ml centrifuge tubes and stored at -20 °C until further analysis.

2.6. SERS sample preparation

In this work, the SERS sample preparation followed that of our previous work [25]. Prior to SERS analysis, 4.5 ml of the gold nanostar colloid was centrifuged at 3500 rpm for 15 min, and the pellet was redispersed in deionised water to remove any excess reactants. The colloid was pre-concentrated by spinning it in a centrifuge and taking out the supernatant until only 100 μl of the colloid was left. The pre-concentrated gold nanostar colloid was briefly sonicated using an ultrasonic sonotrode to homogenise it. Next, 10 μl of the resultant gold colloid was mixed with 9.5 μl of the analyte solution. The mixture was then combined with either 0.5 μl of acidified Na_2SO_4 solution (concentrations ranging from 2 to 0.1 M) as the aggregating agent or 0.5 μl of deionised water as the control. The mixture was vortexed for 2 min at 100 rpm to improve the reproducibility of the SERS spectra [28]. Immediately after

vortexing, the mixture was dropped onto a glass slide wrapped in aluminium foil to reduce interference from the glass slide [29]. Finally, the immersion probe was brought into contact with the liquid droplet, and the SERS spectrum was acquired.

2.7. SERS spectra acquisition and data processing

The Raman spectroscopy setup consisted of a 785 nm narrow linewidth source (XIM-6206-785-500-2, Yixi Intelligent Technology), a high sensitivity spectrometer (YIM-6703-01-S03L01F05G02, Yixi Intelligent Technology), a 785 nm Raman probe (Wasatch Photonics) and a Raman immersion probe with a sapphire ball lens (MarqMetrix). To analyse the SERS spectra, baseline correction and spectral pre-processing were performed using OriginLab Pro (ver. 2022, OriginLab Corporation). The Raman shifts were calibrated to the crystalline silicon peak at 520 cm^{-1} by obtaining the Raman spectrum of silicon wafer and offsetting the Raman shift with the difference between the experimentally obtained crystalline silicon peak and 520 cm^{-1}. All SERS spectra were acquired using a laser power of 100 mW measured at the ball lens of the immersion probe. The integration time for R6G was 5 s, while it was 10 s for lysozyme and grouper epidermal mucus. The lower integration time for R6G was necessary to avoid saturation of the detector. This laser power and integration time did not cause any photodegradation, particularly to the lysozyme protein, as evidenced by the stability of the SERS spectra taken over the course of 90 min shown in figure S3 of the supplementary material. The SERS spectra were smoothened using a wavelet transform with the Debauchies wavelet of order 8 as the mother wavelet and a threshold of 50%. These parameters were chosen because it was observed to reduce noise without merging nearby peaks. Baseline subtraction was conducted using asymmetric least squares smoothing with an asymmetric factor of 0.001, a smoothing factor of 2, a threshold of 0.05 and 10 iterations. The spectra were normalised to the laser emission peak at 0 cm^{-1} and cropped to focus on the fingerprint region between 400 and 1800 cm^{-1}. Subsequently, the baseline for all the spectra was adjusted to zero by subtracting a constant value, determined from the minimum value of each spectrum.

3. Results and discussion

3.1. Characterisation of gold nanostars

The TEM image of the gold nanoparticle seed in figure 1(a) shows that the citrate-capped gold nanoparticles used as the seed for the surfactant-free gold nanostars are fairly homogenous with an average diameter of 16 nm and standard deviation of 1.5 nm, as depicted in figure 1(b).

As shown in figures 2(a) and (b), the formation of gold nanostars was incomplete using 0.5 mM $AgNO_3$ as the shaping agent and when the addition of ascorbic acid was delayed, yielding only anisotropic gold nanoparticles with incompletely formed spikes. Therefore, only gold nanostars synthesised using 1, 2, and 3 mM $AgNO_3$ were used in the subsequent analysis. For ease of discussion, the gold nanostars synthesised using 1, 2, and, 3 mM $AgNO_3$ were labelled S1–S3, respectively.

As evident from the absorbance spectra shown in figure 3, the surface plasmon resonance of the gold nanostars was tuneable by altering the concentration of $AgNO_3$ in the synthesis. The observed red shift of the absorbance peak corresponds to the increase in spike density. S1 has several long and sharp protrusions, while the spikes seen on S3 are dense and short and appear to be more rounded. The hybridisation theory [30] suggests that the broadening of the plasmon peaks is due to the superposition of the core and the tips [31]. From the TEM measurements, the average spike length was measured to be 32, 29, and 27 nm for S1–S3, respectively. Meanwhile, the average aspect ratio of the spikes was measured to be 3.25, 2.42, and 2.2 for S1–S3, respectively.

3.2. SERS of R6G using surfactant-free gold nanostars

The SERS efficiency of the prepared gold nanostars (S1–S3) was first tested with 1 μM R6G solution which is a fluorescent dye with distinct characteristic peaks. Evidently, according to figure 4, S1 yielded the highest enhancement factor. This result indicates that the SERS enhancement favoured gold nanostars with longer spike lengths and higher aspect ratios. Using the peak intensity at 1510 cm^{-1}, the calculated enhancement factor was 4.72×10^6. This value was two orders of magnitude higher compared to the enhancement factor of 1.027×10^4 obtained in our previous work using 44 nm spherical gold nanoparticles (AuNP) [25]. The calculation of the enhancement factor is given in the supplementary material.

The SERS enhancement factor depends on two factors: the coupling of the incident light with the plasmon resonance of the metallic nanostructure and the scattering efficiency [32]. Thus, the total extinction cross-section is the sum of the absorption and scattering cross-section. For smaller nanoparticles and aggregates (<50 nm), the system is accurately characterised by Rayleigh scattering theory. In this regime, the absorption cross-section is dominant, and the enhancement factor is mostly determined by the coupling of the excitation source and the metallic nanostructures's plasmon resonance [33, 34]. However, for larger aggregates (>80 nm), Mie scattering theory becomes more appropriate, where the scattering cross-section is the major factor [35]. Figures 5(a) and (b) show the UV-visible absorption spectra and intensity-size distribution obtained from DLS measurement of the mixture S1–S3 together with 1 mM R6G solution. Figure 5(a) shows that mixing R6G with S2 and S3 shifted the SPR peak closer to the excitation source compared to the S1 mixture. However, the mixing also led to a significant broadening of the SPR peak and a larger hydrodynamic diameter (figure 5(b)), both of which are strong indicators of a high degree of aggregation. Under the Mie scattering regime, the scattering cross-section increases dramatically with the sixth power of the nanoparticle's radius [35]. This phenomenon leads to a decrease in near-field intensity, as more light is

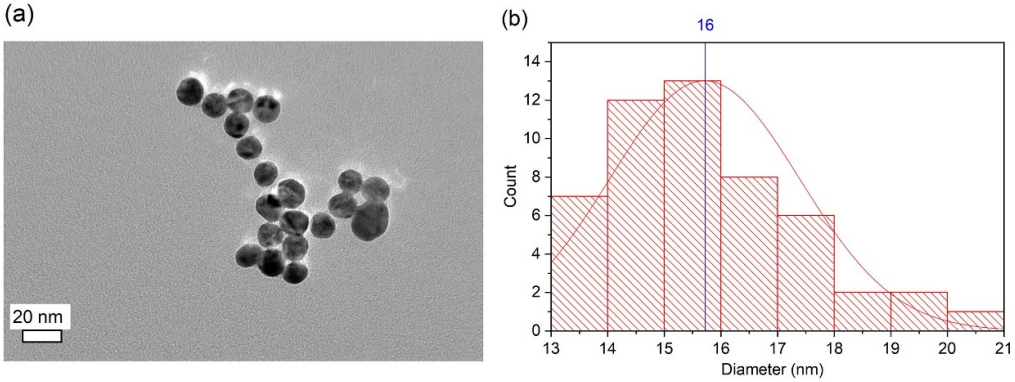

Figure 1. (a) TEM image of the gold nanoparticles seed, where the scale bar denotes 20 nm. (b) Size distribution of 51 gold nanoparticles seed measured from the TEM images.

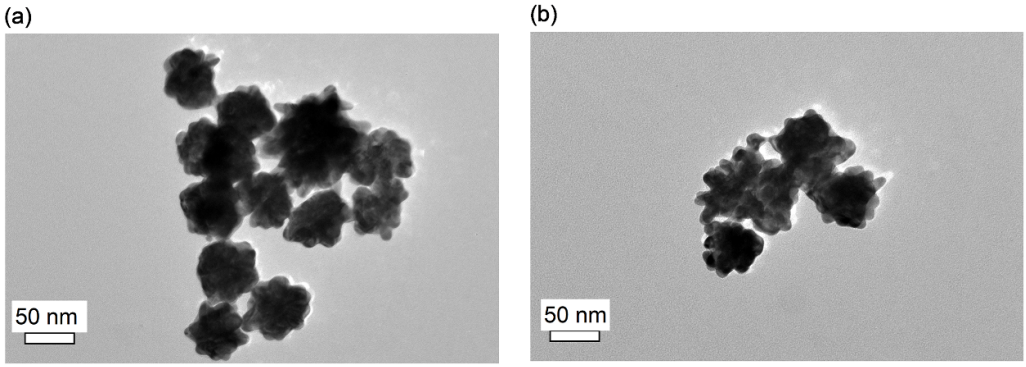

Figure 2. (a) TEM image of gold nanostars synthesised using 0.5 mM $AgNO_3$ as the shaping agent and (b) gold nanostars synthesised using 1 mM $AgNO_3$ as the shaping agent with a 5 s delay for the addition of ascorbic acid.

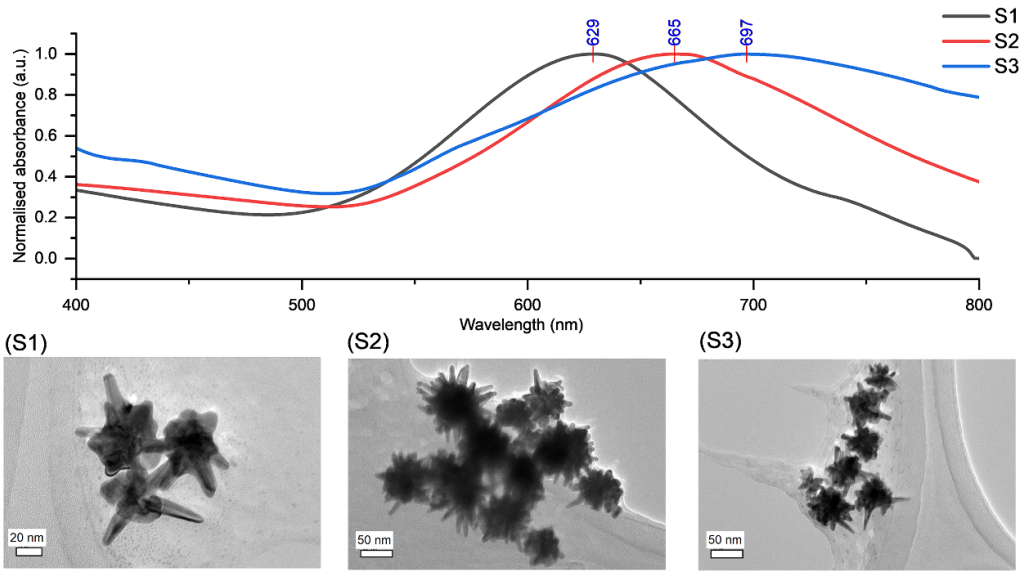

Figure 3. Normalised UV-visible absorbance S1–S3 (top) and TEM images of S1–S3 (bottom). The scale bar represents 20 nm for the image of S1 and 50 nm for the images of S2 and S3.

scattered rather than absorbed to generate the electromagnetic field [35]. While some studies have shown an increase in SERS enhancement as gold nanoparticle size increases within the Rayleigh scattering regime (e.g. from 12 to 25 nm) [36], our results are consistent with the behaviour of larger aggregates. As shown in figure 5(b), the hydrodynamic diameters of our aggregates exceeded 100 nm. The reported works for larger spherical gold nanoparticles demonstrate that SERS enhancement reaches a maximum at a diameter of around 100 nm and then decreases for larger particles [37–39]. Thus, our

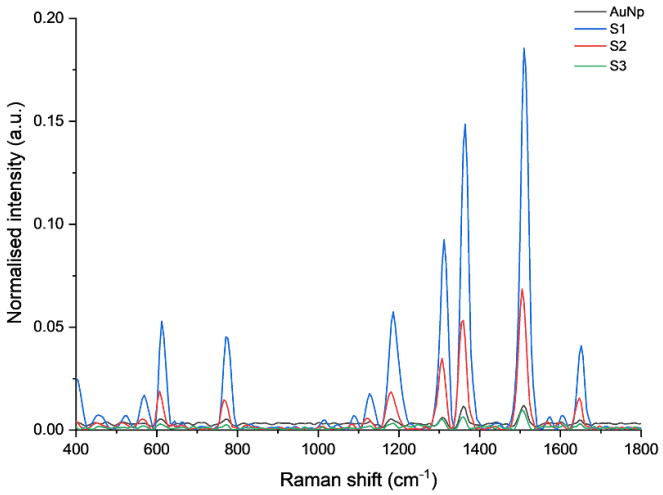

Figure 4. SERS spectra of 1 μM R6G solution obtained using S1–S3 nanostars and spherical AuNp (average diameter of 44 nm).

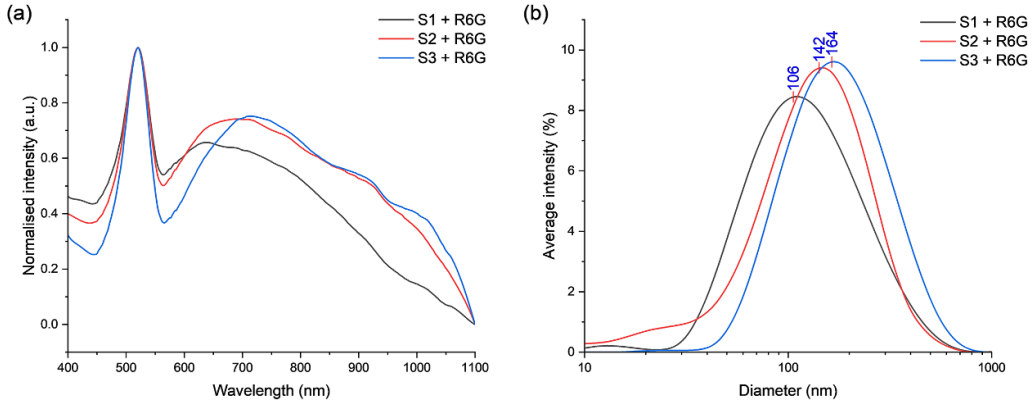

Figure 5. (a) Normalised UV-visible absorbance spectra and (b) intensity-size distribution of the mixture of S1–S3 and 1 mM R6G solution.

finding that the more aggregated S2 and S3 samples exhibited lower SERS enhancement than S1 supports this established principle.

The two mechanisms behind SERS are electromagnetic enhancement and chemical enhancement. Chemical enhancement is a small fraction of the total enhancement, contributing only one or two orders of magnitude, while electromagnetic enhancement can contribute an enhancement factor of 10^6–10^{11} [40]. LSPR [41] and surface plasmon polaritons (SPPs) [42] are understood to play a significant role in forming regions of intense electromagnetic fields, known as 'hot-spots', in the vicinity of metallic nanostructures which contribute to signal enhancement. In a colloidal system, these hot-spots are originated from the aggregation of nanoparticles in the colloid. Inorganic salts are typically added to nanoparticles colloids to induce aggregation by destabilising the electric double layer of the suspended nanoparticles. This reduces the zeta potential and interparticle repulsion, consequently shortening the interparticle distance and encouraging the coupling of LSPR and SPPs of adjacent nanoparticles [43].

In this study, acidified Na_2SO_4 solution (pH 3) was used as the aggregating agent due to the weak affinity of the sulphate ion on the silver surface, which reduces competitive binding [44, 45]. The affinity of sulphate ion on the gold surface is hypothesised to be similar. In addition, sulphate ions also cause a greater degree of destabilisation of the surface charge on gold nanoparticle surfaces compared to chloride and nitrate ions [43]. Furthermore, the acidic pH maintains the mixture below the isoelectric point of most proteins. This condition ensures that the proteins, including lysozyme and those in the epidermal mucus, have a nett positive charge and thus adsorb on the gold nanoparticle surface via electrostatic attraction [46]. Figure 6 shows the SERS spectra of R6G solution obtained using Na_2SO_4 with concentration ranging from 0.1 to 2 M as the aggregating agent. The results indicated that unaggregated gold nanostars produced the best SERS enhancement. Fales and Vo-Dinh [47] also reported the higher SERS performance of silver-embedded gold nanostars in the unaggregated state. The unique geometry of gold nanostars may provide sufficient SERS hot-spots in the unaggregated state, and salt-induced aggregation may cause the broadening

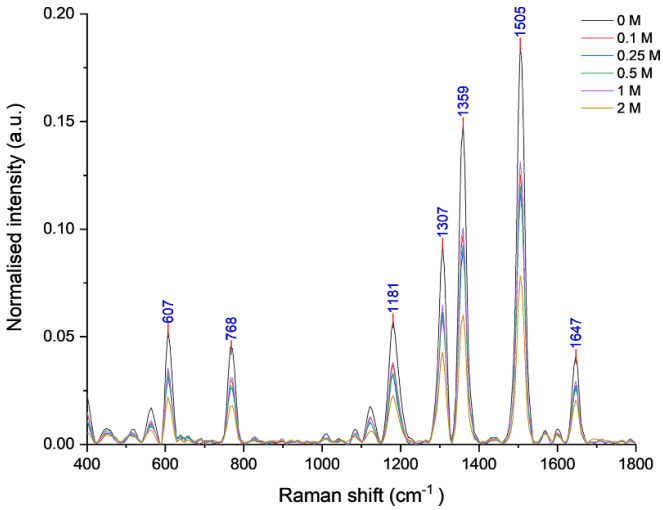

Figure 6. SERS spectra of 1 μM R6G solution with S1 in the presence of various concentrations of Na_2SO_4 solution.

Table 1. Peak assignment of R6G. The peak values are assigned within ± 5 cm^{-1} of the literature value to account for instrumental differences.

Peak (cm^{-1})	Functional group	References
607	C–C–C in-plane bending	[49]
768	C–H out-of-plane bending	[50]
1181	C–H in-plane bending, in-plane xanthene ring deformation, N–H bending	[49]
1307	In-plane xanthene ring bending, N–H bending, CH_2 wagging	[51]
1359	Xanthene ring stretch, C–H in-plane bending	[49]
1505	Xanthene ring stretch, C–N stretching, C–H and N–H bending	[49]
1647	Xanthene ring stretch, C–H in-plane bending	[50]

of the LSPR peak which may be detuned from the excitation laser wavelength, causing the diminished SERS performance in the aggregated state [48]. The peak assignment is summarised in table 1.

3.3. SERS of lysozyme and grouper epidermal mucus using surfactant-free gold nanostars

Based on the results in figures 4 and 6, the SERS performance of gold nanostars was significantly better than spherical gold nanoparticles. However, the enhancement was only observed in S1, which has fewer but longer spikes. Evidently, the enhancement is dependent on the morphology of the gold nanostars. Therefore, similar investigation was done on 300 μg ml^{-1} lysozyme protein solution and grouper epidermal mucus, which is a complex matrix consisting of a wide range of biomolecules.

Based on figure 7(a), S1 exhibited the highest enhancement factor, outperforming the spherical gold nanoparticles. Similar to the observation with R6G, the peak intensities using S1 decreased upon the addition of the aggregating agent, as shown in figure 7(b). Interestingly, S2 and S3 did not produce any discernible peaks. Proteins adsorbed on gold nanoparticle surfaces tend to unfold due to strong intermolecular interactions between the gold nanoparticle and protein, which may destabilise the internal interactions in the protein molecule responsible for the secondary and tertiary structure of the protein [52]. Protein unfolding on the gold nanoparticle surface leads to the formation of gold nanoparticle-protein aggregates [53]. Further aggregation through the introduction of Na_2SO_4 may form large aggregates which shield some of the adsorbed lysozyme proteins from the excitation laser [54], which may explain the results shown in figure 7(b). Moreover, aggregation of gold nanoparticles causes a red-shift and broadening of the SPR peak [55], which may explain the dramatic decrease in SERS performance of S2 and S3. The peak assignment for lysozyme is summarised in table 2.

Figures 8(a) and (b) show the UV-visible absorption spectra and intensity-size distribution, respectively, obtained from triplicate DLS measurements of the mixture of S1–S3 together with lysozyme. The broadening and red-shifting of the SPR peak are clearly visible in figure 8(a). Similar to the SERS analysis of R6G, the SPR peaks of the mixture of S2, S3, and lysozyme are closer to the excitation source. However, S2 and S3 formed larger aggregates upon interaction with lysozyme, evidenced by the larger hydrodynamic diameter shown

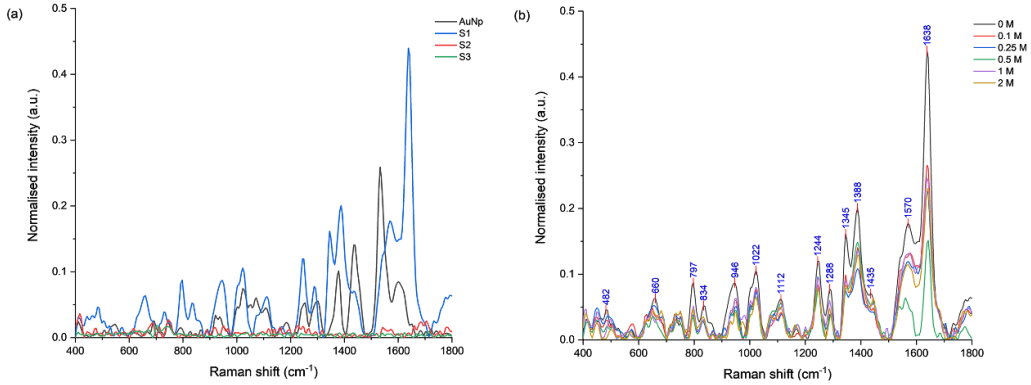

Figure 7. (a) SERS spectra of lysozyme obtained using AuNp, S1–S3 and the SERS spectra of lysozyme obtained using S1 and with the addition of various concentrations of Na_2SO_4 as the aggregating agent is shown in (b). The identified peaks are marked in (b).

Table 2. Peak assignment for the SERS spectrum of lysozyme. The peak values are assigned within ± 5 cm^{-1} of the literature values to account for instrumental differences.

Peak (cm^{-1})	Functional group	References
482	S–S	[56]
660	C–S stretch, tyrosine	[57]
797	C–H stretch, N–H deformation	[57]
834	Tyrosine	[58]
946	C–C stretching of the α-helical structure	[59]
1022	Phenylalanine, β-sheet	[57–59]
1112	C–N, C=S	[57, 60]
1244	Amide III	[58]
1288	Amide III	[58]
1345	Tryptophan, CH_2 and CH_3 deformation	[57, 58]
1388	CH_3 deformation	[60]
1435	CH_2 deformation	[57]
1570	Amide II	[57]
1638	Amide I	[57, 59]

in figure 8(b). The obtained results exhibited aggregates' diameters of greater than 140 nm, which indicate that the aggregates fall within the Mie scattering theory regime. The significantly higher scattering cross-section of these larger aggregates leads to a decrease in the intensity of the localised electric field and consequently, a decreased SERS enhancement factor [35].

The Raman spectrum of proteins have several distinct bands arising from the polypeptide backbone, namely, amide A, B and I to VII [59]. Amongst these bands, the amide I band (1600–1700 cm^{-1}), corresponding to the C=O stretch of the polypeptide backbone, is particularly useful for characterising protein secondary structure. The amide I envelope is the superposition of the various C=O stretching frequencies due to the unique geometry of proteins and hydrogen bonds within the protein molecule [61]. Figure 9 shows the unenhanced Raman spectrum and SERS spectra of 300 μg ml^{-1} of lysozyme (Lyz) between 1500 and 1800 cm^{-1}. The unenhanced Raman spectrum is shown as the black trace, while the SERS spectra obtained using the spherical gold nanoparticles in our previous work [25] and S1 are shown as the red and blue trace, respectively, in figure 9. This region contains both the amide II (1500–1600 cm^{-1}) and amide I (1600–1700 cm^{-1}). However, the amide II band is less sensitive and selective to protein conformational changes [61]. Therefore, the spectra in figure 9 were normalised to the amide II peak.

Typically, the SERS spectrum of proteins exhibits a suppression of the amide I band, an effect attributed to the shielding of the polypeptide backbone from the gold nanoparticle surface by the amino acid side chains [41]. This was observed in the red trace in figure 9. However, the amide I suppression was not observed on the spectrum obtained using S1 (blue trace), as shown in figure 9. The enhancement factor for lysozyme obtained using S1 was calculated to be 7.62×10^5 relative to the intensity of the amide I peak of the unenhanced Raman spectrum of lysozyme. This indicates the unique geometry of the gold nanostars was able to enhance both the polypeptide backbone and the amino acid side chains. However, the absence of the peak in the region between 1649 and 1660 cm^{-1} on both the red and blue traces in figure 9 suggests a conformational change from α-helical structure to β-sheets [41]. Additionally, figure 9 also shows the higher degree of conformational changes in the lysozyme protein adsorbed on the AuNp surface compared to S1. This can be seen from the blue-shifting of the amide I and amide II peaks from 1633 to 1602 cm^{-1} and 1556–1533 cm^{-1}, respectively, indicating a

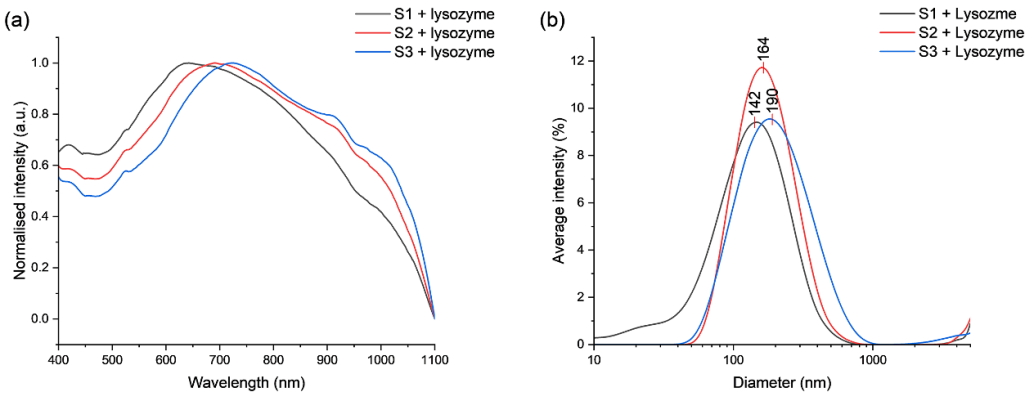

Figure 8. (a) UV-visible absorption spectra and (b) intensity-size distribution of the mixture of S1–S3 and 300 μg ml^{-1} lysozyme solution.

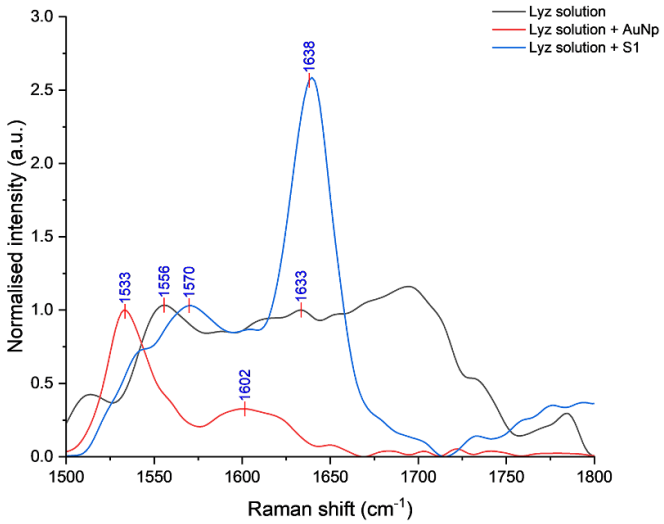

Figure 9. Raman spectrum (black), SERS spectrum obtained using spherical gold nanoparticle (red) and S1 nanostars (blue) of 300 μg ml^{-1} lysozyme solution. The spectra are normalised to the amide II peak centred around 1550 cm^{-1}. The Raman spectrum was obtained using the same parameters as the SERS spectra without the addition of gold nanoparticles. The amide I and II peaks are labelled in each spectrum.

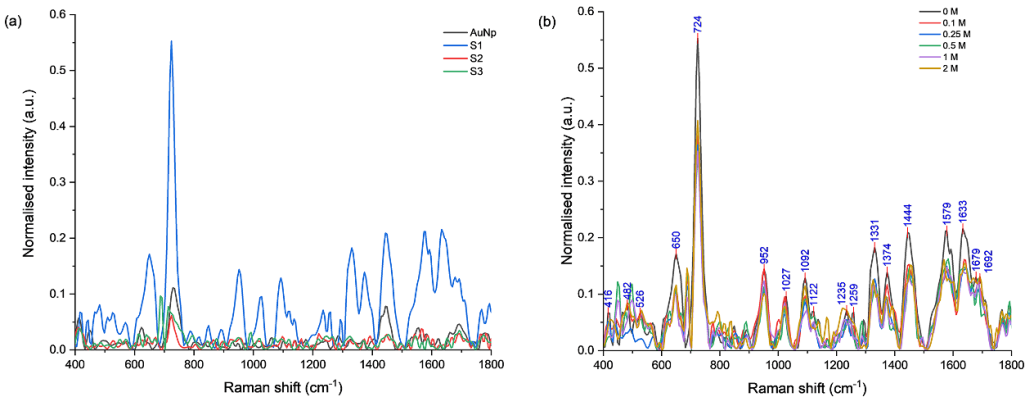

Figure 10. (a) SERS spectra of grouper epidermal mucus obtained using AuNp, S1–S3. The SERS spectra of grouper epidermal mucus obtained using S1 with the addition of various concentrations of Na_2SO_4 are shown in (b). The identified peaks are marked in (b).

conformational change to a secondary structure with more β-sheets [62].

Based on figures 10(a) and (b), the enhancement factor was the highest using S1 and in the absence of Na_2SO_4 as the aggregating agent. Coupled with the results shown in figures 4, 6 and 7, it is evident that the SERS performance was the best for all the analytes using S1 without the addition of Na_2SO_4 as the aggregating agent. These results clearly indicate the SERS

Table 3. Tentative peak assignment of the SERS spectrum of grouper epidermal mucus. The peaks are assigned within ± 5 cm^{-1} of the literature values to account for instrumental differences.

Peak (cm^{-1})	Functional group	Tentative peak assignment	Ref.erences
416	Aliphatic C–C chain deformation	Tryptophan	[57, 60, 64]
482, 526	S–S stretch	Cystine	[60, 65]
650	Aliphatic C–S stretch, ring deformation	Methionine, tyrosine	[57, 58, 65]
724	Aliphatic C–S stretch, indole ring breathing	Methionine, tryptophan	[60, 64, 65]
952	C–C stretch of α-helical structure	Proteins	[55, 57, 58]
1027	Benzene ring breathing	Phenylalanine	[58, 65]
1092	C–C, C–N stretch and ring bending	Proteins	[57]
1122	C–N stretching	Proteins, valine	[58, 66]
1235	Amide III	Proteins	[58, 59]
1259	Amide III, α-helical structure	Proteins	[59]
1331	C–H aliphatic deformation, ring stretching	Proteins, tryptophan	[58, 64, 65]
1374	CH_3 symmetric deformation	Proteins, alanine	[57, 65]
1444	CH_2 deformation	Proteins, glycine	[57, 65]
1579	Indole ring, NH_2 scissoring	Proteins, tryptophan	[57, 67]
1633	Amide I, β-sheet	Proteins	[61]
1679, 1692	Amide I, β-turn	Proteins	[61]

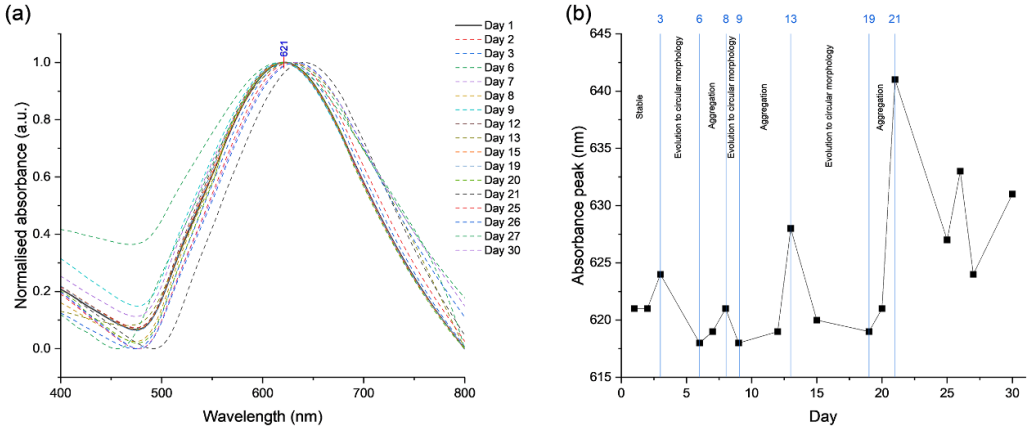

Figure 11. (a) Normalised UV-visible absorbance spectra of S1 measured over 30 days and (b) the progression of the SPR peak over 30 days. The spectra after the day 1 are drawn with dashed lines in (a) for visual clarity.

enhancement is dependent on the morphology of the gold nanostars and the enhancement favours the gold nanostars with fewer but longer spikes. In addition, the SERS performance of the gold nanostars was the best in the unaggregated state.

Grouper epidermal mucus is a complex matrix consisting of a wide variety of immune related compounds such as antimicrobial peptides, lysozymes, lectins, and proteases which play vital roles in fish physiology [23]. Therefore, the constituents of the epidermal mucus reflect changes in fish physiology. However, the SERS spectrum of epidermal mucus is the superposition of all the compounds in the epidermal mucus, which makes the identification of the individual compounds difficult. The functional group and the tentative peak assignment of the peaks identified in figure 10(b) is summarised in table 3. Despite this, in our previous work, differences in peak intensity between the control group and experimental group were able to reveal the differences in physiological response to hypoxia in hypoxia-tolerant and intolerant fish [63]. Based on figure 10(a), the sensitivity of S1 for in-solution SERS was significantly higher than the 44 nm spherical gold nanoparticles used in both of our previous works [25, 63].

3.4. Stability of the gold nanostars and repeatability of the synthesis

The gold nanostars synthesised in the presence of 1 mM $AgNO_3$ (S1) were found to be the best morphology to obtain the highest enhancement factor. Figures 11(a) and (b) show UV-visible absorbance spectra measured over 30 days and the progression of the SPR peak of S1 respectively. Due to the lack of stabilising ligands, the stability of the surfactant-free gold nanostars was poor. Based on figure 11(b), S1 was stable up to the second day after synthesis. The red-shift in the SPR peak indicates the formation of aggregates, and the blue-shift indicates an evolution to a more circular morphology and the blunting of the spikes. Figure 11(b) shows that there was a cycle of aggregation followed by blunting of the spikes over the course of 30 days. Figure 12 clearly shows that

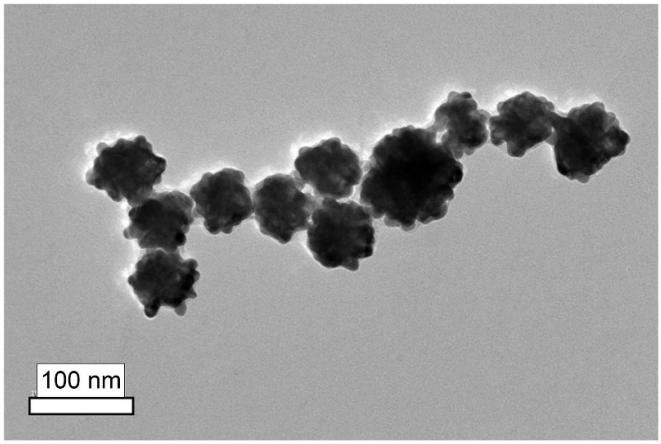

Figure 12. TEM image of S1 after 7 days post synthesis.

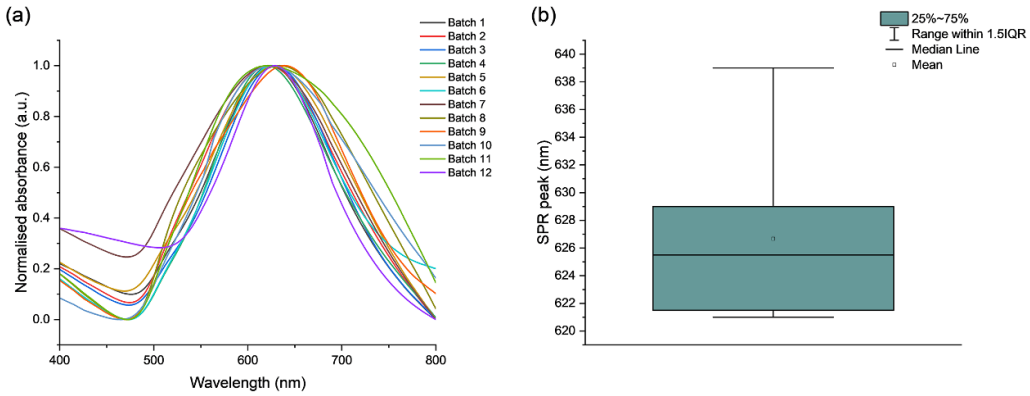

Figure 13. (a) UV-visible absorbance of 12 batches of S1 and (b) box plot of the SPR peak.

the morphology becomes more circular and the spikes have become significantly blunt seven days after synthesis.

The repeatability of the synthesis was also investigated. Twelve batches of S1 were prepared on the same day, and the UV-visible absorbance spectra of the twelve batches are shown in figure 13(a) and from the box plot in figure 13(b), the mean SPR peak was 635 nm with standard error of 2.54 nm and a standard deviation of 9.16 nm. The small standard error and standard deviation indicate that the synthesis is repeatable. The variation in FWHM, however, may be due to the different average spike lengths in each synthesis.

3.5. *Effects of stabilising ligands*

Sodium citrate and potassium iodide (KI) were tested as stabilising ligands for gold nanostars. Both citrate ions and iodide ions are negatively charged, and the adsorption of the ions on the gold nanostars' surface provides a layer of negative charge. Two batches of S1 were incubated with 100 μl of 1 mM sodium citrate and potassium iodide solution overnight. The resulting colloids were centrifuged and redispersed in 10 ml of deionised water to remove any unbound citrate and iodide ions. The electrostatic repulsion of the negatively charged ions on the surface prevents the aggregation of the gold nanostars, but there was a significant reduction of the enhancement factor due to competitive binding, as evident in figure 14. The citrate capping appears to have a slightly better enhancement factor compared to the iodide capping, possibly due to the lower affinity of citrate ions to gold surfaces. However, in the interest of obtaining the highest enhancement factor for the best signal

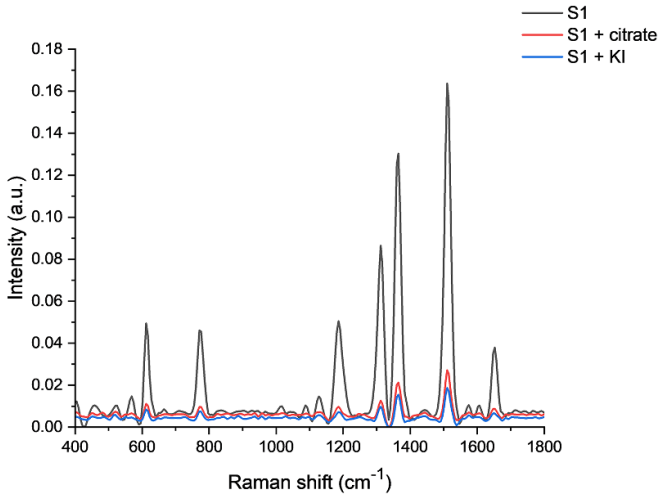

Figure 14. SERS spectra of R6G obtained using bare gold nanostars, citrate capped and iodide capped gold nanostars.

quality, the addition of stabilising ligands was not pursued further. In this work, the gold nanostars were synthesised at most a day prior to conducting SERS analysis.

4. Conclusion

This study demonstrates that surfactant-free gold nanostars are a highly viable colloidal substrate for SERS in biological fluids. The surfactant-free synthesis route utilises silver ions to tune morphology and the resulting SPR peaks. Our results show that gold nanostars synthesised with 1 mM $AgNO_3$ (S1) exhibited the most effective morphology, characterised by a high aspect ratio of 3.25. This structure, with long spikes, proved to be superior for in-solution SERS, yielding the highest enhancement factors for all tested analytes; R6G, lysozyme, and grouper epidermal mucus. Specifically, enhancement factors of 4.72×10^6 for R6G and 7.62×10^5 for lysozyme were achieved with these unaggregated nanostars. Furthermore, the low enhancement factor of S2 and S3 is due to the higher degree of aggregation, leading to the increased light scattering, which lowers the localised electromagnetic field intensity. These gold nanostars are also capable of enhancing protein polypeptide backbone peaks, which are typically shielded from enhancement. While the surfactant-free route provides high SERS activity, it introduces a colloidal instability that causes aggregation and spike blunting just a few days post-synthesis. Note that these nanostars lacked stabilising ligands to preserve their SERS-active morphology. Future work will focus on improving stability without compromising the enhancement factor, building upon our finding that gold nanostars with fewer, longer spikes in an unaggregated state offer superior performance. This study provides a strong foundation for unlocking new insights into biological analyses using SERS.

Data availability statement

The SERS spectra will be made available upon request from the corresponding author.

The data cannot be made publicly available upon publication because they contain commercially sensitive information. The data that support the findings of this study are available upon reasonable request from the authors.

Enhancement factor and stability available at https://doi.org/10.1088/1361-6528/ae0ada/data1.

Ethics approval

This study used hybrid groupers (*Epinephelus fuscoguttatus* × *Epinephelus lanceolatus*). Prior to the experimentation, the proposal for this study was reviewed and approved by the Institutional Animal Care and Use Committee, Universiti Putra Malaysia (UPM/ACUC/AUP-R054/2022).

Funding

This research work is fully funded by the Ministry of Higher Education, Malaysia under the Transdisciplinary Research Grant Scheme (TRGS/1/2020/UPM/02/1/1) and the King Saud University, Kingdom of Saudi Arabia, under the Ongoing Research Funding Program (ORF-2025-336).

Conflict of interest

The authors declare no competing interests.

Author contributions

Nathaniel Leong
Formal analysis (lead), Investigation (lead), Visualization (lead), Writing – original draft (lead)

Chou Min Chong 0000-0003-3440-505X
Supervision (equal), Writing – review & editing (equal)

Annie Christianus 0000-0001-8577-386X
Supervision (equal)

Zuraidah Zan 0000-0002-9385-1925
Supervision (equal)

Mohammed Thamer Alresheedi 0000-0001-8477-2902
Funding acquisition (lead), Writing – review & editing (equal)

Norita Mohd Yusoff 0000-0003-2122-8664
Resources (lead)

Mohd Hanif Yaacob 0000-0002-3026-3202
Conceptualization (lead), Methodology (lead)

Mohd Adzir Mahdi 0000-0002-2843-181X
Funding acquisition (lead), Project administration (lead), Supervision (lead), Writing – review & editing (lead)

References

[1] Smith E and Dent G 2005 *Modern Raman Spectroscopy—a Practical Approach* (Wiley)
[2] Crocombe R A 2018 Portable spectroscopy *Appl. Spectrosc.* **72** 1701–51
[3] Butler H J *et al* 2016 Using Raman spectroscopy to characterize biological materials *Nat. Protocol* **11** 664–87
[4] Das G, Mecarini F, Gentile F, De Angelis F, Mohan Kumar H, Candeloro P, Liberale C, Cuda G and Di Fabrizio E 2009 Nano-patterned SERS substrate: application for protein analysis vs. temperature *Biosens. Bioelectron.* **24** 1693–9
[5] Kho K W, Shen Z X, Zeng H C, Soo K C and Olivo M 2005 Deposition method for preparing SERS-active gold nanoparticle substrates *Anal. Chem.* **77** 7462–71
[6] Zhang C, Chen S, Jiang Z, Shi Z, Wang J and Du L 2021 Highly sensitive and reproducible SERS substrates based on ordered micropyramid array and silver nanoparticles *ACS Appl. Mater. Interfaces* **13** 29222–9

[7] Știufiuc G F *et al* 2020 Solid plasmonic substrates for breast cancer detection by means of SERS analysis of blood plasma *Nanomaterials* **10** 1212

[8] Mercadal P A, Encina E R, Villa J E L and Coronado E A 2021 A new figure of merit to assess the SERS enhancement factor of colloidal gold nanoparticle aggregates *J. Phys. Chem. C* **125** 4056–65

[9] Martinez E J C, Rodriguez-Villalon O, Cordova T, Perez-Careta E, Guzmán-Sepúlveda J R, Madrid-Molina L and Guzman-Cabrera R 2020 Quantitative pharmaceutical analysis based on the PCA of Raman spectra *Rev. Chim.* **71** 347–54

[10] Vilela D, González M C and Escarpa A 2012 Sensing colorimetric approaches based on gold and silver nanoparticles aggregation: chemical creativity behind the assay. A review *Anal. Chim. Acta* **751** 24–43

[11] Mahmoud A Y F, Rusin C J and McDermott M T 2020 Gold nanostars as a colloidal substrate for in-solution SERS measurements using a handheld Raman spectrometer *Analyst* **145** 1396–407

[12] Bibikova O, Haas J, López-Lorente Á I, Popov A, Kinnunen M, Ryabchikov Y, Kabashin A, Meglinski I and Mizaikoff B 2017 Surface enhanced infrared absorption spectroscopy based on gold nanostars and spherical nanoparticles *Anal. Chim. Acta* **990** 141–9

[13] Becerril-Castro I B, Calderon I, Pazos-Perez N, Guerrini L, Schulz F, Feliu N, Chakraborty I, Giannini V, Parak W J and Alvarez-Puebla R A 2022 Gold nanostars: synthesis, optical and SERS analytical properties *Anal. Sens.* **2** e202200005

[14] Liebig F, Henning R, Sarhan R M, Prietzel C, Schmitt C N Z, Bargheer M and Koetz J 2019 A simple one-step procedure to synthesise gold nanostars in concentrated aqueous surfactant solutions *RSC Adv.* **9** 23633–41

[15] Vu S V, Nguyen A-T, Tran A-T C, Le V-H T, Lo T N H, Ho T H, Pham N N T, Park I and Vo K Q 2023 Differences between surfactant-free Au@Ag and CTAB-stabilized Au@Ag star-like nanoparticles in the preparation of nanoarrays to improve their surface-enhanced Raman scattering (SERS) performance *Nanoscale Adv.* **5** 5543–61

[16] Zhang Y, Newton B, Lewis E, Fu P P, Kafoury R, Ray P C and Yu H 2015 Cytotoxicity of organic surface coating agents used for nanoparticles synthesis and stability *Toxicol. Vitro* **29** 762–8

[17] Bibikova O *et al* 2016 plasmon-resonant gold nanostars with variable size as contrast agents for imaging applications *IEEE J. Sel. Top Quantum Electron.* **22** 13–20

[18] Yuan H, Khoury C G, Hwang H, Wilson C M, Grant G A and Vo-Dinh T 2012 Gold nanostars: surfactant-free synthesis, 3D modelling, and two-photon photoluminescence imaging *Nanotechnology* **23** 75102

[19] Chatterjee S, Ringane A B, Arya A, Das G M, Dantham V R, Laha R and Hussian S 2016 A high-yield, one-step synthesis of surfactant-free gold nanostars and numerical study for single-molecule SERS application *J. Nanopart. Res.* **18** 242

[20] Harder R A, Wijenayaka L A, Phan H T and Haes A J 2021 Tuning gold nanostar morphology for the SERS detection of uranyl *J. Raman Spectrosc.* **52** 497–505

[21] Lin M-H, Sun L, Kong F and Lin M 2021 Rapid detection of paraquat residues in green tea using surface-enhanced Raman spectroscopy (SERS) coupled with gold nanostars *Food Control* **130** 108280

[22] Zaccone G, Kapoor B G, Fasulo S and Ainis L 2001 Structural, histochemical and functional aspects of the epidermis of fishes *Adv. Mar. Biol.* **40** 253–348

[23] Dash S, Das S K, Samal J and Thatoi H N 2018 Epidermal mucus, a major determinant in fish health: a review *Iran. J. Vet. Res.* **19** 72–81

[24] Nurhikmah, Christianus A, Wan Solahudin W M S, Lau W M, Ismail B Y and Fei L C 2022 Skin mucus proteome analysis reveals disease-resistant biomarker signatures in hybrid grouper (*Epinephelus fuscoguttatus* ♀ × *Epinephelus lanceolatus* ♂) against vibrio alginolyticus *Fishes* **7** 278

[25] Leong N, Yaacob M H, Zain A R M, Aziz T H T A, Christianus A, Chong C M and Mahdi M A 2024 Colloidal surface-enhanced Raman spectroscopic study of grouper epidermal mucus using acidified sodium sulphate as the aggregating agent *Spectrochim. Acta A* **311** 123974

[26] Turkevich J, Stevenson P C and Hillier J 1951 A study of the nucleation and growth processes in the synthesis of colloidal gold *Discuss. Faraday Soc.* **11** 55–75

[27] Ramsey J D, Zhou L, Kyle Almlie C, Lange J D and Burrows S M 2015 Achieving plasmon reproducibility from surfactant free gold nanostar synthesis *New J. Chem.* **39** 9098–108

[28] Tantra R, Brown R J C and Milton M J T 2007 Strategy to improve the reproducibility of colloidal SERS *J. Raman Spectrosc.* **38** 1469–79

[29] Cui L, Butler H J, Martin-Hirsch P L and Martin F L 2016 Aluminium foil as a potential substrate for ATR-FTIR{,} transflection FTIR or Raman spectrochemical analysis of biological specimens *Anal. Methods* **8** 481–7

[30] Hao F, Nehl C L, Hafner J H and Nordlander P 2007 Plasmon resonances of a gold nanostar *Nano Lett.* **7** 729–32

[31] Khoury C G and Vo-Dinh T 2008 Gold nanostars for surface-enhanced Raman scattering: synthesis, characterization and optimization *J. Phys. Chem. C* **112** 18849–59

[32] Yamamoto Y S and Itoh T 2016 Why and how do the shapes of surface-enhanced Raman scattering spectra change? Recent progress from mechanistic studies *J. Raman Spectrosc.* **47** 78–88

[33] Jain P K, Lee K S, El-Sayed I H and El-Sayed M A 2006 Calculated absorption and scattering properties of gold nanoparticles of different size, shape, and composition: applications in biological imaging and biomedicine *J. Phys. Chem. B* **110** 7238–48

[34] Truong P L, Ma X and Sim S J 2014 Resonant Rayleigh light scattering of single Au nanoparticles with different sizes and shapes *Nanoscale* **6** 2307–15

[35] Kelly K L, Coronado E, Zhao L L and Schatz G C 2003 The optical properties of metal nanoparticles: the influence of size, shape, and dielectric environment *J. Phys. Chem. B* **107** 668–77

[36] Alam Md S, Tanvir N I, Moniruzzaman M, Shaikh M A A and Farhad S F U 2024 Size variant spherical gold nanoparticles for *in situ* detection of trace contaminants by surface enhanced Raman spectroscopy *MRS Adv.* **9** 1345–51

[37] Njoki P N, Lim I-I S, Mott D, Park H-Y, Khan B, Mishra S, Sujakumar R, Luo J and Zhong C-J 2007 Size correlation of optical and spectroscopic properties for gold nanoparticles *J. Phys. Chem. C* **111** 14664–9

[38] López-Tobar E, Hernández B, Chenal A, Coïc Y-M, Gómez Santos J, Mejía-Ospino E, Garcia-Ramos J V, Ghomi M and Sanchez-Cortes S 2017 Large size citrate-reduced gold colloids appear as optimal SERS substrates for cationic peptides *J. Raman Spectrosc.* **48** 30–37

[39] Zhang P, Li Y, Wang D and Xia H 2016 High-yield production of uniform gold nanoparticles with sizes from 31 to 577 nm via one-pot seeded growth and size-dependent SERS property *Part. Part. Syst. Charact.* **33** 924–32

[40] Xie L, Lu J, Liu T, Chen G, Liu G, Ren B and Tian Z 2020 Key role of direct adsorption on SERS sensitivity: synergistic effect among target, aggregating agent, and surface with Au or Ag colloid as surface-enhanced raman spectroscopy substrate *J. Phys. Chem. Lett.* **11** 1022–9

[41] Kurouski D, Large N, Chiang N, Greeneltch N, Carron K T, Seideman T, Schatz G C and Duyne R P V 2016 Unraveling near-field and far-field relationships for 3D SERS substrates—a combined experimental and theoretical analysis *Analyst* **141** 1779–88
[42] Mohaghegh F, Tehrani A M and Materny A 2021 Investigation of the importance of the electronic enhancement mechanism for surface-enhanced Raman scattering (SERS) *J. Phys. Chem. C* **125** 5158–66
[43] Mostowtt T, Munoz J and McCord B 2019 An evaluation of monovalent, divalent, and trivalent cations as aggregating agents for surface enhanced Raman spectroscopy (SERS) analysis of synthetic cannabinoids *Analyst* **144** 6404–14
[44] Bell S E J, Mackle J N and Sirimuthu N M S 2005 Quantitative surface-enhanced Raman spectroscopy of dipicolinic acid–towards rapid anthrax endospore detection *Analyst* **130** 545–9
[45] Bell S E J and Sirimuthu N M S 2005 Surface-enhanced Raman spectroscopy as a probe of competitive binding by anions to citrate-reduced silver colloids *J. Phys. Chem. A* **109** 7405–10
[46] Han X X, Huang G G, Zhao B and Ozaki Y 2009 Label-free highly sensitive detection of proteins in aqueous solutions using surface-enhanced Raman scattering *Anal. Chem.* **81** 3329–33
[47] Fales A M and Vo-Dinh T 2015 Silver embedded nanostars for SERS with internal reference (SENSIR) *J. Mater. Chem. C* **3** 7319–24
[48] Chegel V, Rachkov O, Lopatynskyi A, Ishihara S, Yanchuk I, Nemoto Y, Hill J P and Ariga K 2012 Gold nanoparticles aggregation: drastic effect of cooperative functionalities in a single molecular conjugate *J. Phys. Chem. C* **116** 2683–90
[49] Shi G, Han X, Gu J, Yuan W, Li K, Wang L, Han W and Gu J 2022 Ag nanoislands modified carbon fiber nanostructure: a versatile and ultrasensitive surface-enhanced raman scattering platform for antiepileptic drug detection *Coatings* **12** 4
[50] He X N, Gao Y, Mahjouri-Samani M, Black P N, Allen J, Mitchell M, Xiong W, Zhou Y S, Jiang L and Lu Y F 2012 Surface-enhanced Raman spectroscopy using gold-coated horizontally aligned carbon nanotubes *Nanotechnology* **23** 205702
[51] Hildebrandt P and Stockburger M 1984 Surface-enhanced resonance Raman spectroscopy of rhodamine 6G adsorbed on colloidal silver *J. Phys. Chem.* **88** 5935–44
[52] Franco R and Pereira E 2013 Gold nanoparticles and proteins, interaction *Encyclopedia of Metalloproteins* ed R H Kretsinger, V N Uversky and E A Permyakov (Springer) pp 908–15
[53] Zhang D, Neumann O, Wang H, Yuwono V M, Barhoumi A, Perham M, Hartgerink J D, Wittung-Stafshede P and Halas N J 2009 Gold nanoparticles can induce the formation of protein-based aggregates at physiological pH *Nano Lett.* **9** 666–71
[54] Turzhitsky V, Zhang L, Horowitz G L, Vitkin E, Khan U, Zakharov Y, Qiu L, Itzkan I and Perelman L T 2018 Picoanalysis of drugs in biofluids with quantitative label-free surface-enhanced Raman spectroscopy *Small* **14** 1–11
[55] Neupane S, Pan Y, Takalkar S, Bentz K, Farmakes J, Xu Y, Chen B, Liu G, Qian S Y and Yang Z 2017 Probing the aggregation mechanism of gold nanoparticles triggered by a globular protein *J. Phys. Chem. C* **121** 1377–86
[56] Biswas N, Waring A J, Walther F J and Dluhy R A 2007 Structure and conformation of the disulfide bond in dimeric lung surfactant peptides SP-B1-25 and SP-B8-25 *Biochim. Biophys. Acta* **1768** 1070–82
[57] Szekeres G P and Kneipp J 2019 SERS probing of proteins in gold nanoparticle agglomerates *Front. Chem.* **7** 1–10
[58] Rygula A, Majzner K, Marzec K M, Kaczor A, Pilarczyk M and Baranska M 2013 Raman spectroscopy of proteins: a review *J. Raman Spectrosc.* **44** 1061–76
[59] Li-Chan E, Nakai S and Hirotsuka M 1994 Raman spectroscopy as a probe of protein structure in food systems *Protein Structure-Function Relationships in Foods* ed R Y Yada, R L Jackman and J L Smith (Springer) pp 163–97
[60] Yvon H J 2017 Raman spectroscopy for analysis and monitoring *Horiba Jobin Yvon, Raman Application Note* pp 1–2 (available at: www.horiba.com/fileadmin/uploads/Scientific/Documents/Raman/bands.pdf)
[61] Sadat A and Joye I J 2020 Peak fitting applied to Fourier transform infrared and Raman spectroscopic analysis of proteins *Appl. Sci.* **10** 5918
[62] Krimm S and Bandekar J 1986 Vibrational spectroscopy and conformation of peptides, polypeptides, and proteins *Advances in Protein Chemistry* vol 38, ed C B Anfinsen, J T Edsall and F M Richards (Academic) pp 181–364
[63] Leong N, Mujar E K, Mazlan A N, Chong C M, Christianus A, Alresheedi M T, Ng E K, Yaacob M H and Mahdi M A 2025 Discrimination of hypoxia tolerant and intolerant hybrid groupers using surface-enhanced Raman spectroscopy of epidermal mucus *Aquaculture* **598** 742014
[64] Chuang C-H and Chen Y-T 2009 Raman scattering of L-tryptophan enhanced by surface plasmon of silver nanoparticles: vibrational assignment and structural determination *J. Raman Spectrosc.* **40** 150–6
[65] Zhu G, Zhu X, Fan Q and Wan X 2011 Raman spectra of amino acids and their aqueous solutions *Spectrochim. Acta A* **78** 1187–95
[66] Podstawka-Proniewicz E, Andrzejak M, Kafarski P, Kim Y and Proniewicz L M 2011 Vibrational characterization of L-valine phosphonate dipeptides: FT-IR, FT-RS, and SERS spectroscopy studies and DFT calculations *J. Raman Spectrosc.* **42** 958–79
[67] Maiti N, Thomas S, Jacob J A, Chadha R, Mukherjee T and Kapoor S 2012 DFT and surface-enhanced Raman scattering study of tryptophan–silver complex *J. Colloid Interface Sci.* **380** 141–9